

In situ characterization of battery materials using x-ray absorption spectroscopy

Carlo Segre

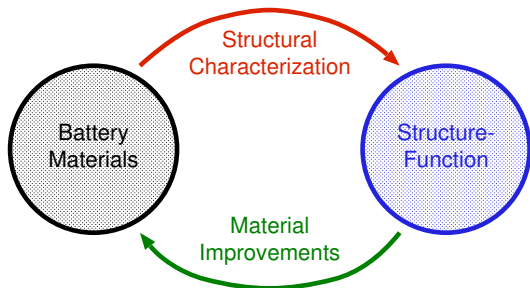
Physics Department
&
Center for Synchrotron Radiation Research and Instrumentation
Illinois Institute of Technology

May 22, 2018



- Motivation
- XAS experiments at MRCAT
- Application of XAS to batteries
- In situ Ni@Co core shell cathode
- Sn_4P_3 /graphite composite anode
- A look to the future

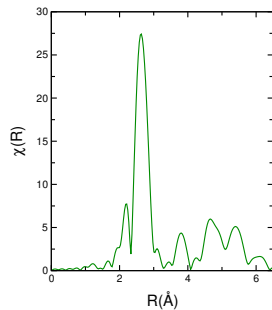
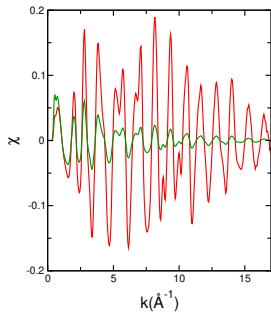
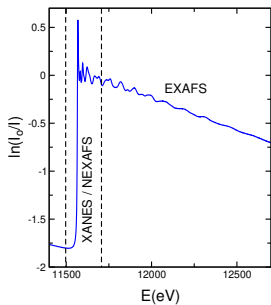
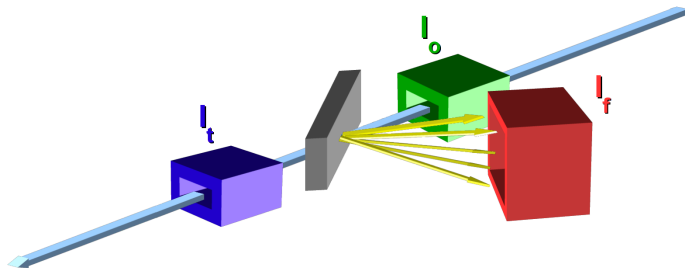
Why x-ray absorption spectroscopy?



X-ray absorption spectroscopy provides element-specific view of both crystalline and amorphous phases with time resolution relevant to battery studies

Ideal for study of degradation mechanisms and structural reversibility

The XAS experiment





Cathode materials:

- Ni(OH)₂@Co(OH)₂
- MnO₂
- LiCoO₂
- Li_{1.2}(NiMnCo)_{0.8}O₂
- Li_{1.2}(MnNiFe)_{0.8}O₂
- Li₃V₂(PO₄)₃
- LiFePO₄

Edge	Energy
Li	0.055 keV
V	5.465 keV
Mn	6.539 keV
Fe	7.112 keV
Co	7.709 keV
Ni	8.333 keV

Li edge not directly accessible and 3d element energies challenging for *in situ* experiments (must use fluorescence).

Anode materials:

- Fe₂O₃
- ZnO
- MoS₂
- Sn
- SnO₂
- Sn₃O₂(OH)₂
- Sn₄P₃

Edge	Energy
P	2.145 keV
S	2.472 keV
Fe	7.112 keV
Zn	9.659 keV
Mo	20.00 keV
Sn	29.20 keV

P and S edges too low for non-vacuum experiments, Zn, Fe good in fluorescence, Mo and Sn ideal for *in situ* experiments.



ID Line

XAFS (4 keV - 65 keV)

Continuous scan (< 1 min)

Very dilute samples

BM Line

XAFS (4 keV - 32 keV)

Continuous scan (~ 4 min)

SDD for dilute samples



ID Line

XAFS (4 keV - 65 keV)

Continuous scan (< 1 min)

Very dilute samples

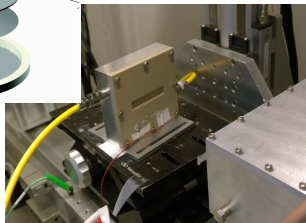
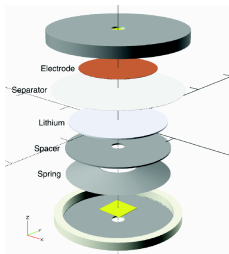
BM Line

XAFS (4 keV - 32 keV)

Continuous scan (~ 4 min)

SDD for dilute samples





ID Line

XAFS (4 keV - 65 keV)

Continuous scan (< 1 min)

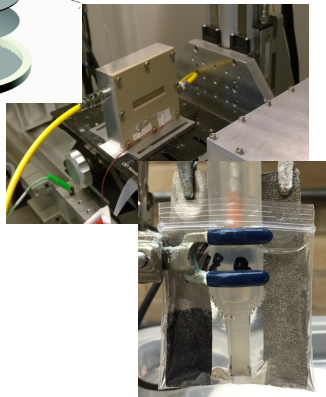
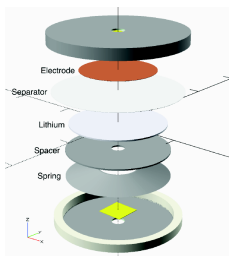
Very dilute samples

BM Line

XAFS (4 keV - 32 keV)

Continuous scan (\sim 4 min)

SDD for dilute samples



ID Line

XAFS (4 keV - 65 keV)

Continuous scan (< 1 min)

Very dilute samples

BM Line

XAFS (4 keV - 32 keV)

Continuous scan (\sim 4 min)

SDD for dilute samples



ID Line

XAFS (4 keV - 65 keV)

Continuous scan (< 1 min)

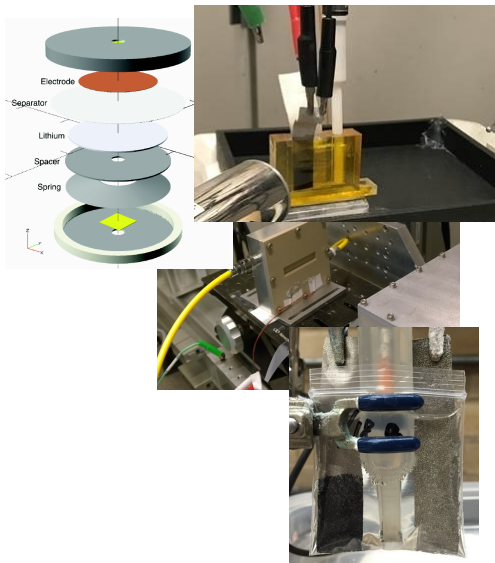
Very dilute samples

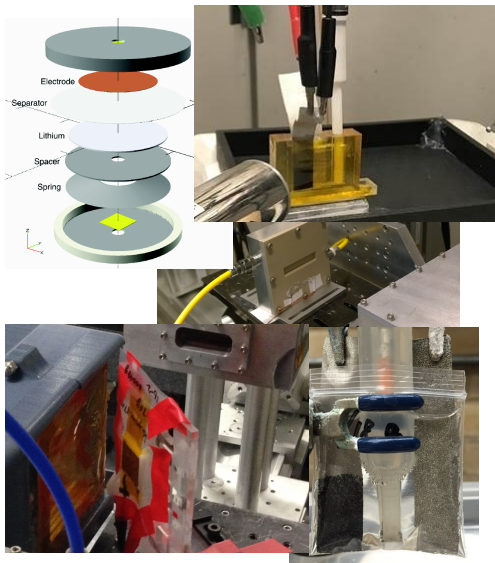
BM Line

XAFS (4 keV - 32 keV)

Continuous scan (\sim 4 min)

SDD for dilute samples





ID Line

XAFS (4 keV - 65 keV)

Continuous scan (< 1 min)

Very dilute samples

BM Line

XAFS (4 keV - 32 keV)

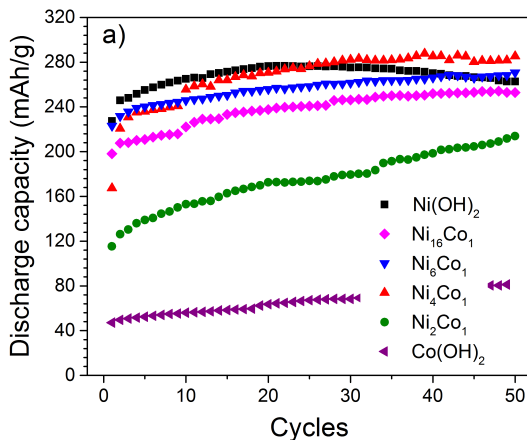
Continuous scan (~ 4 min)

SDD for dilute samples

Ni(OH)₂ for nanofluid flow cathodes



Co(OH)₂ is a common additive to Ni(OH)₂ cathode materials



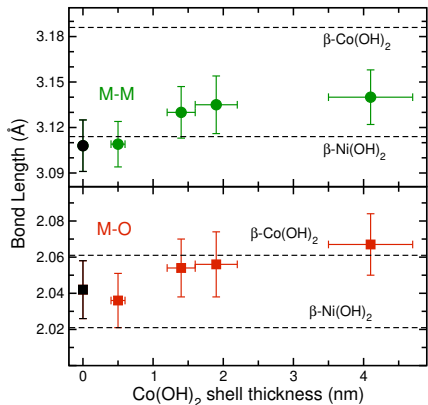
Co(OH)₂ improves electrical conductivity but is not considered to contribute to the reversible capacity

Coat Ni(OH)₂ nanoparticles with varying thickness of Co(OH)₂

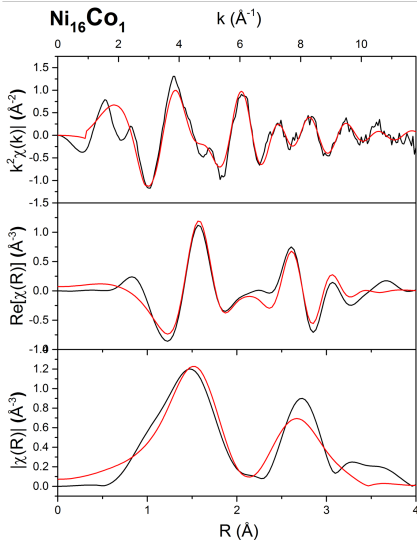
Optimal Co(OH)₂ coating shows nearly theoretical pure Ni(OH)₂ capacity

E. Moazzen, E.V. Timofeeva, and C.U Segre, "Role of crystal lattice templating and galvanic coupling in enhanced reversible capacity of Ni(OH)₂/Co(OH)₂ core/shell battery cathode," *Electrochim. Acta* **258**, 684-693 (2017).

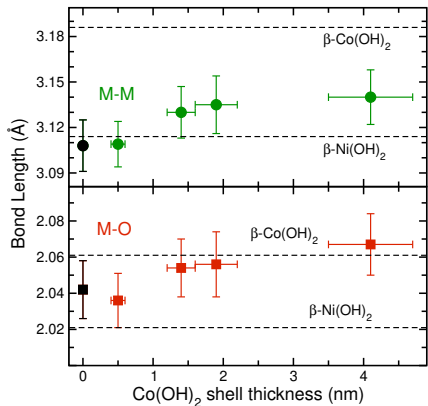
Ni(OH)₂@Co(OH)₂ templating



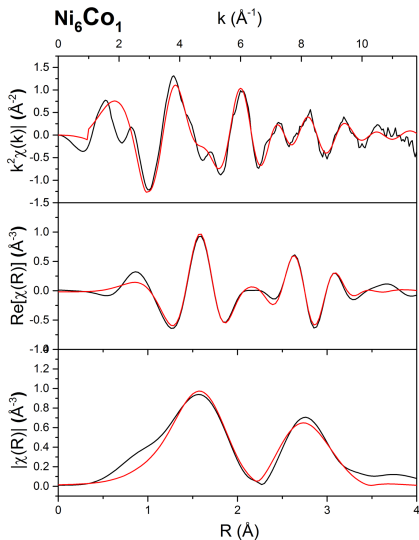
EXAFS points to Co(OH)₂ templating
not discernible with x-ray diffraction



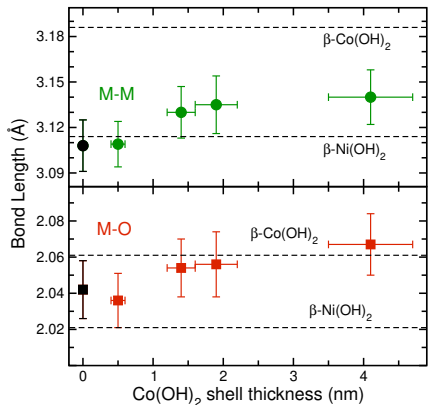
Ni(OH)₂@Co(OH)₂ templating



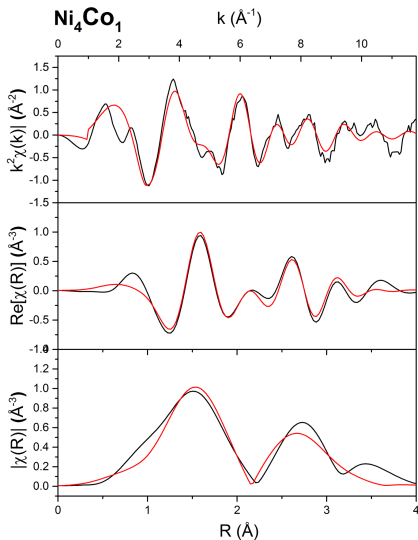
EXAFS points to Co(OH)₂ templating
not discernible with x-ray diffraction



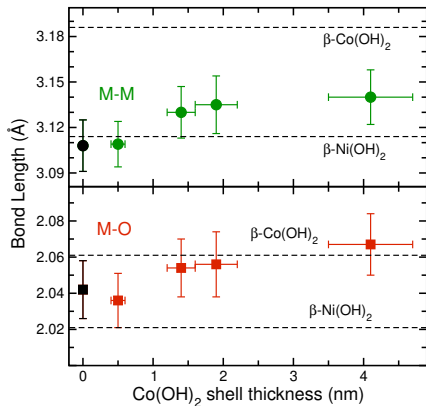
Ni(OH)₂@Co(OH)₂ templating



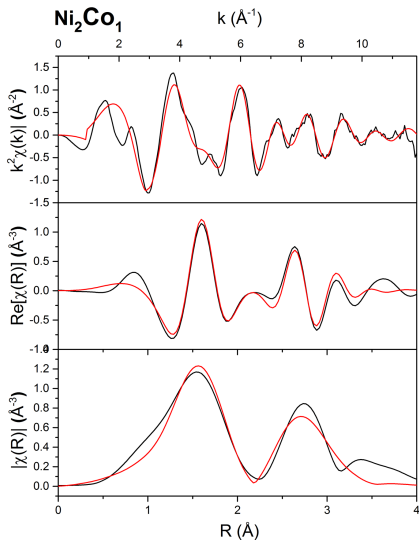
EXAFS points to Co(OH)₂ templating
not discernible with x-ray diffraction



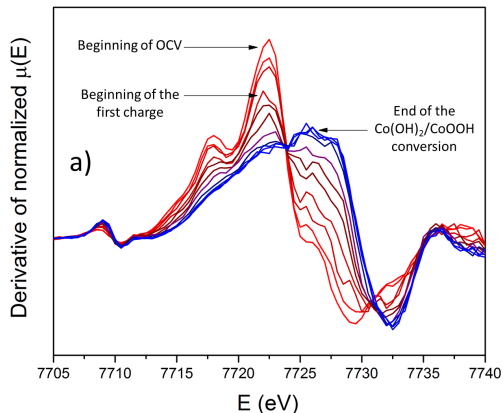
Ni(OH)₂@Co(OH)₂ templating



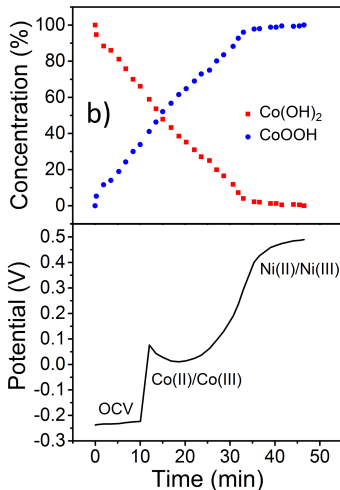
EXAFS points to Co(OH)₂ templating
not discernible with x-ray diffraction



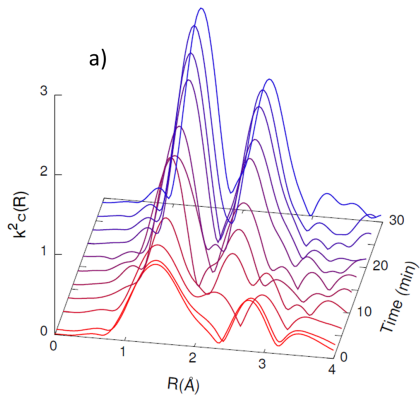
Ni(OH)₂@Co(OH)₂ in situ XANES



Oxidation of Co(OH)_2 begins even before charging current is applied

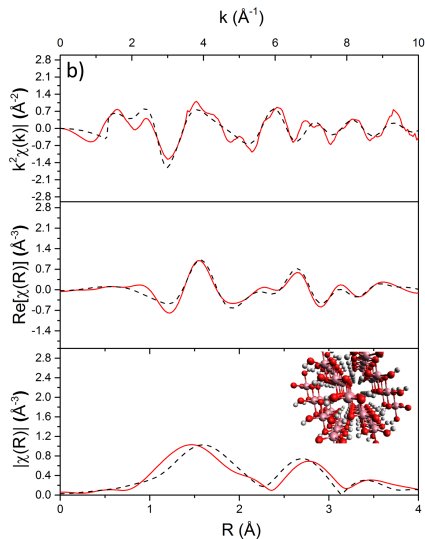


Ni(OH)₂@Co(OH)₂ in situ EXAFS

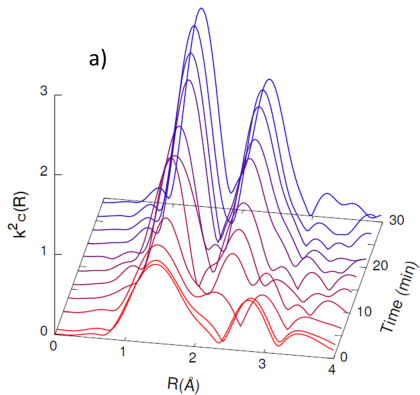


All fits performed with single parameter and endpoint spectra

Oxidized state shows shorter and more ordered Co-O bonds

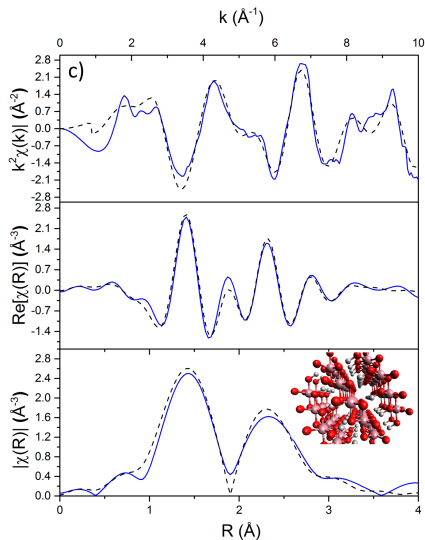


Ni(OH)₂@Co(OH)₂ in situ EXAFS

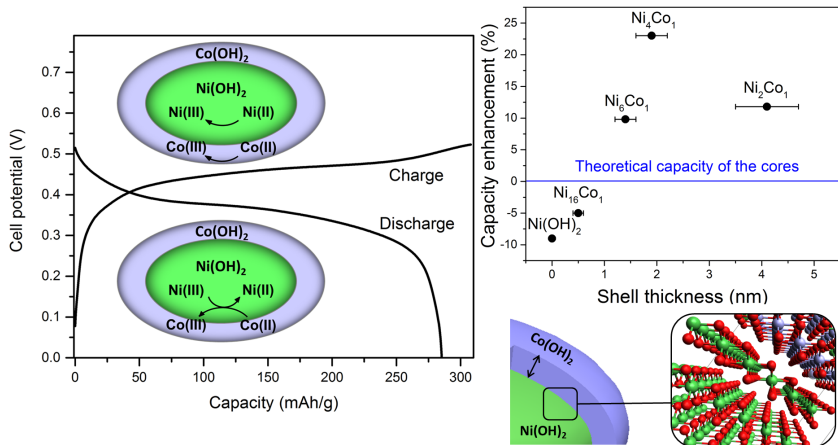


All fits performed with single parameter and endpoint spectra

Oxidized state shows shorter and more ordered Co-O bonds

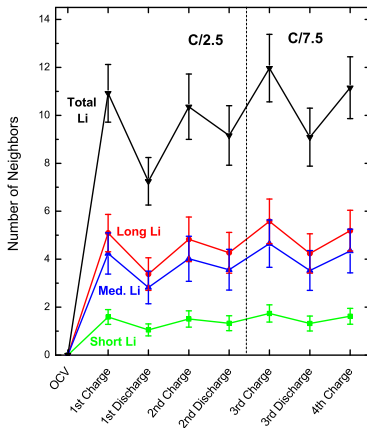
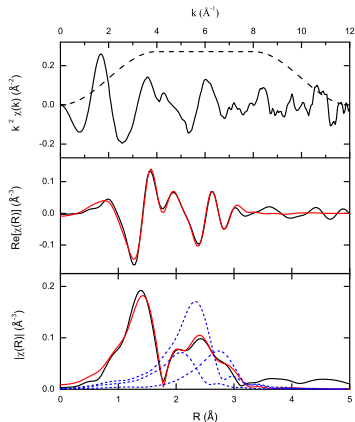


Ni(OH)₂@Co(OH)₂ galvanic couple



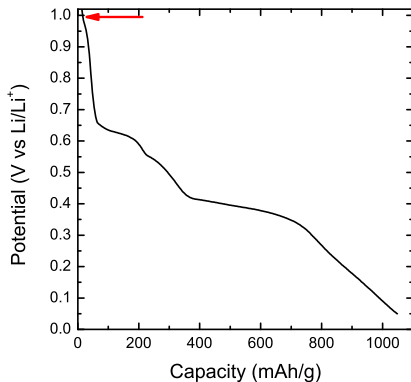
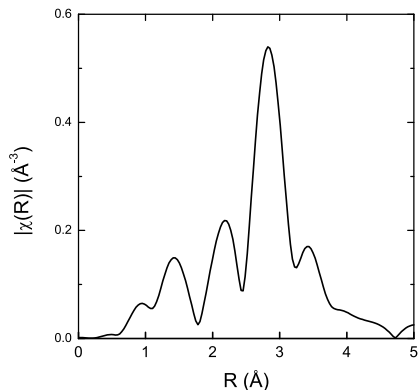
E. Moazzen, E.V. Timofeeva, and C.U Segre, "Role of crystal lattice templating and galvanic coupling in enhanced reversible capacity of Ni(OH)₂/Co(OH)₂ core/shell battery cathode," *Electrochim. Acta* **258**, 684-693 (2017).

Initial *in situ* Sn-based anode EXAFS

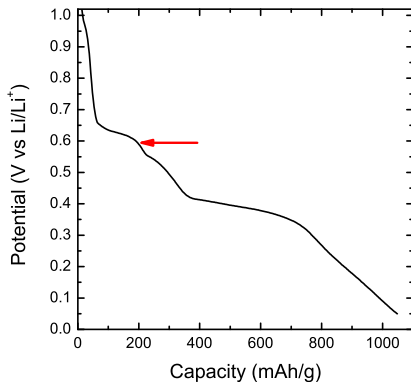
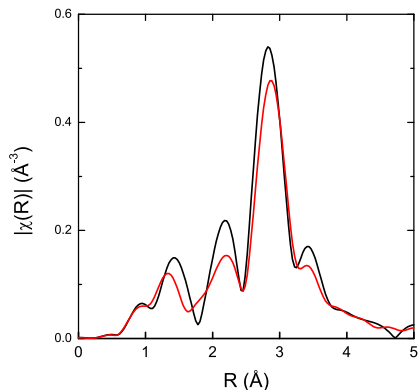


$\text{Li}_{22}\text{Sn}_5$ has 14 Sn-Li paths with distance of 3.4 \AA or less. Model with three Sn-Li paths at “center of mass” locations

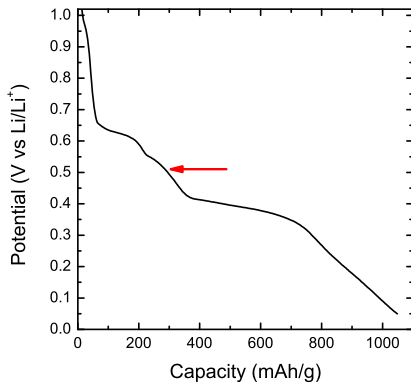
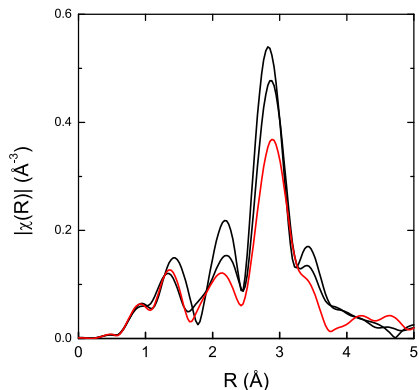
C. Pelliccione, E.V. Timofeeva, and C.U. Segre, “In situ XAS study of the capacity fading mechanism in hybrid $\text{Sn}_3\text{O}_2(\text{OH})_2$ /graphite battery anode nanomaterials”, *Chem. Mater.* **27**, 574-580 (2015).



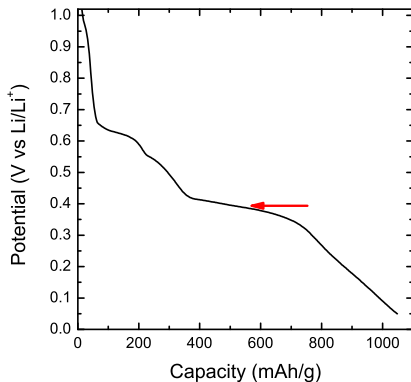
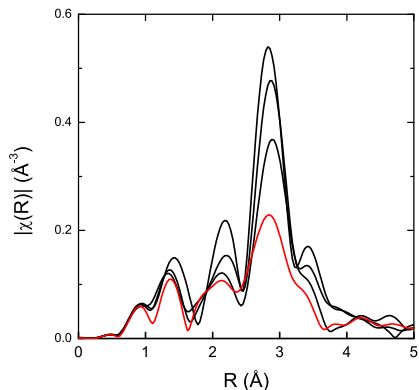
C.J. Pelliccione, E.V. Timofeeva, and C.U. Segre, "Potential-resolved in situ x-ray absorption spectroscopy study of Sn and SnO_2 nanomaterial anodes for lithium-ion batteries," *J. Phys. Chem. C* **120**, 5331-5339 (2016).



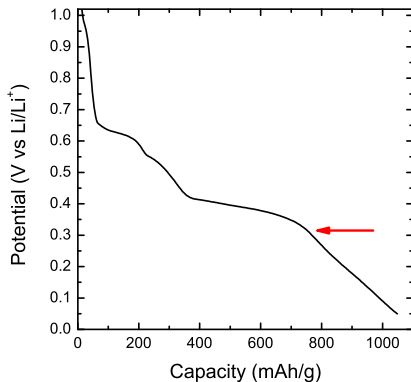
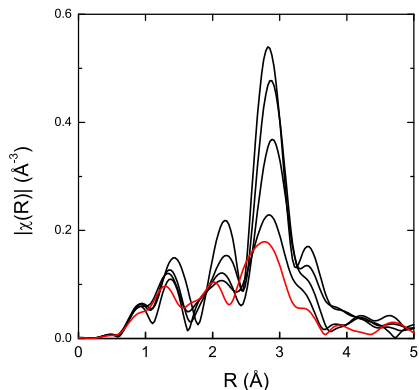
C.J. Pelliccione, E.V. Timofeeva, and C.U. Segre, "Potential-resolved in situ x-ray absorption spectroscopy study of Sn and SnO₂ nanomaterial anodes for lithium-ion batteries," *J. Phys. Chem. C* **120**, 5331-5339 (2016).



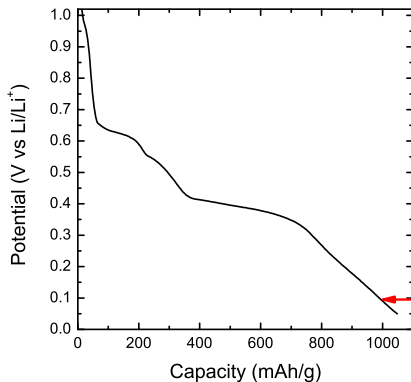
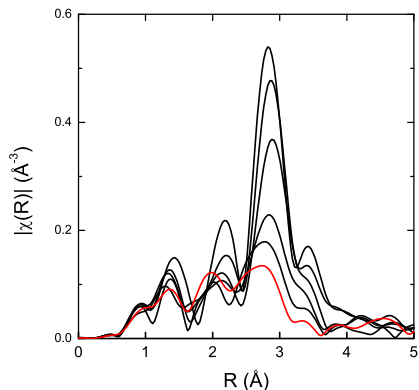
C.J. Pelliccione, E.V. Timofeeva, and C.U. Segre, "Potential-resolved in situ x-ray absorption spectroscopy study of Sn and SnO_2 nanomaterial anodes for lithium-ion batteries," *J. Phys. Chem. C* **120**, 5331-5339 (2016).



C.J. Pelliccione, E.V. Timofeeva, and C.U. Segre, "Potential-resolved in situ x-ray absorption spectroscopy study of Sn and SnO_2 nanomaterial anodes for lithium-ion batteries," *J. Phys. Chem. C* **120**, 5331-5339 (2016).

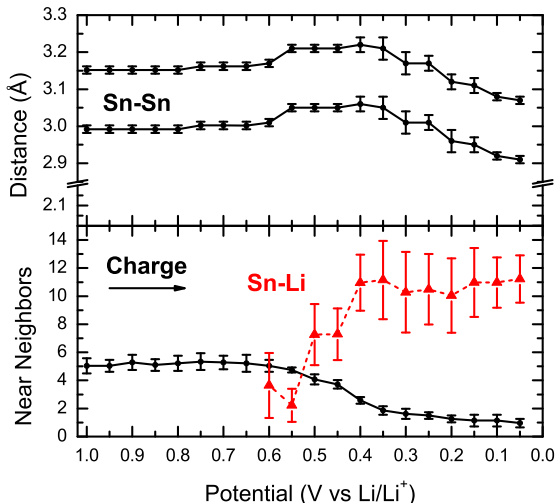


C.J. Pelliccione, E.V. Timofeeva, and C.U. Segre, "Potential-resolved in situ x-ray absorption spectroscopy study of Sn and SnO_2 nanomaterial anodes for lithium-ion batteries," *J. Phys. Chem. C* **120**, 5331-5339 (2016).



C.J. Pelliccione, E.V. Timofeeva, and C.U. Segre, "Potential-resolved in situ x-ray absorption spectroscopy study of Sn and SnO₂ nanomaterial anodes for lithium-ion batteries," *J. Phys. Chem. C* **120**, 5331-5339 (2016).

The Sn lithiation process



0.60V – Sn metal begins to break down and Li appears

0.45V – number of Li reaches 11 and stabilizes at near full Li₂₂Sn₅

However, Sn fades rapidly due to electric conductivity loss. What can be improved?

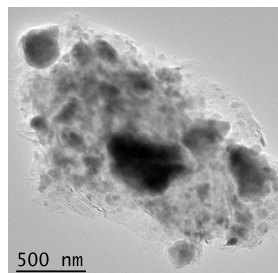
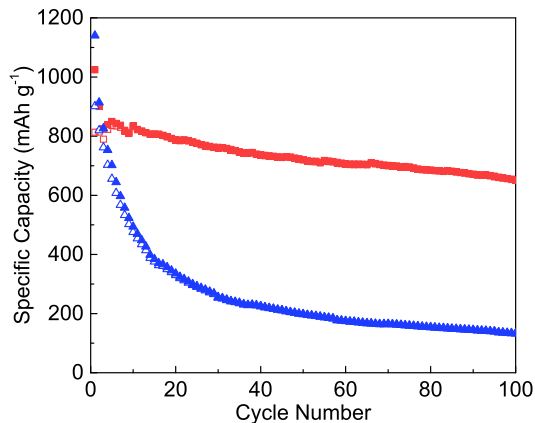
C.J. Pelliccione, E.V. Timofeeva, and C.U. Segre, "Potential-resolved in situ x-ray absorption spectroscopy study of Sn and SnO₂ nanomaterial anodes for lithium-ion batteries," *J. Phys. Chem. C* **120**, 5331-5339 (2016).

Sn₄P₃/graphite composite anode



Sn₄P₃ synthesized by high energy ball milling, then ball milled again with graphite to obtain composite

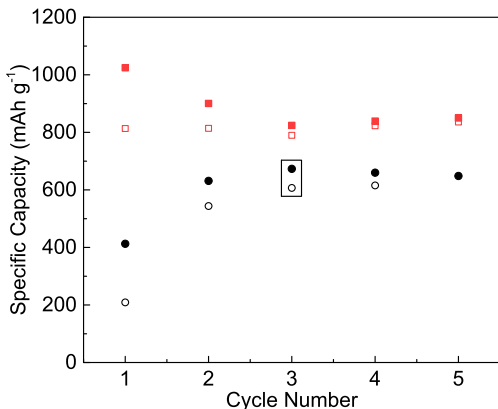
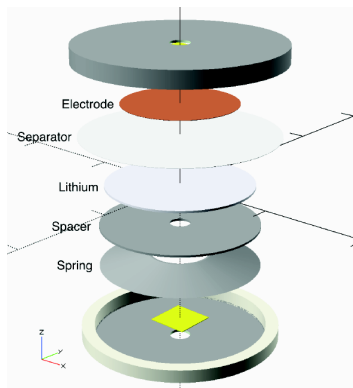
Theoretically could transfer 9 or more electrons upon lithiation



Sn₄P₃/graphite composite shows stable, reversible capacity of 610 mAh/g for 100 cycles at C/2 compared to rapidly fading pure Sn₄P₃ material.

How does the lithiation process differ from that of Sn metal?

In situ EXAFS of Sn₄P₃/graphite

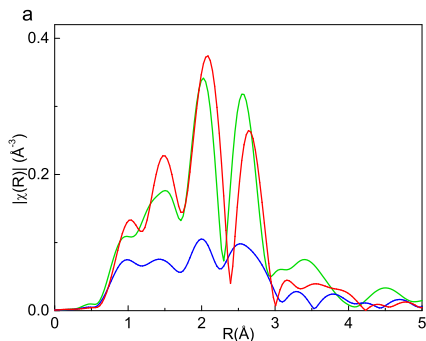


Results for *in situ* coin cell are close to the capacity of the unmodified cell at C/4, indicating good reversibility by the 3rd cycle.

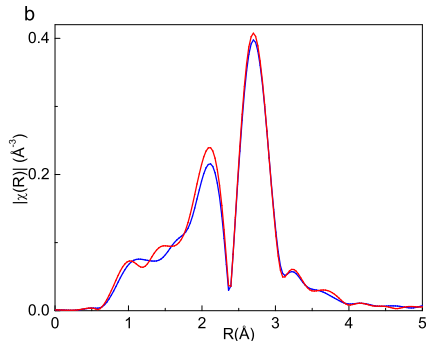
Third cycle comparison



By the **third lithiation** and **third delithiation**, the difference between pure Sn_4P_3 and the Sn_4P_3 /graphite composite is clear.



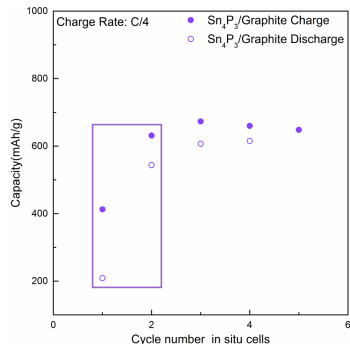
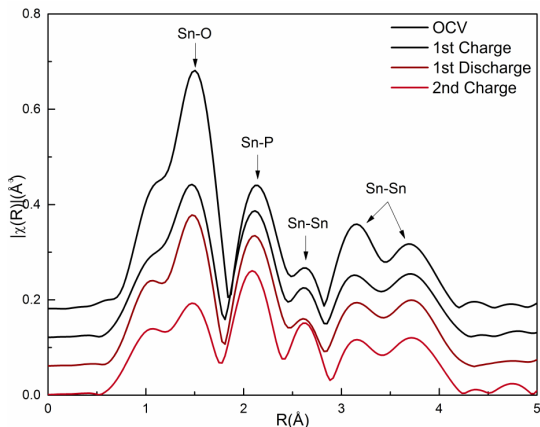
Sn_4P_3 /graphite composite



pure Sn_4P_3

Even at the **100th delithiation**, the Sn_4P_3 /graphite composite measured *ex situ* is showing the same features as at the 3rd cycle.

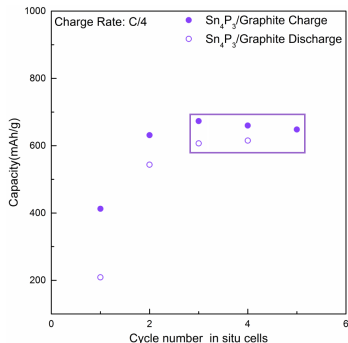
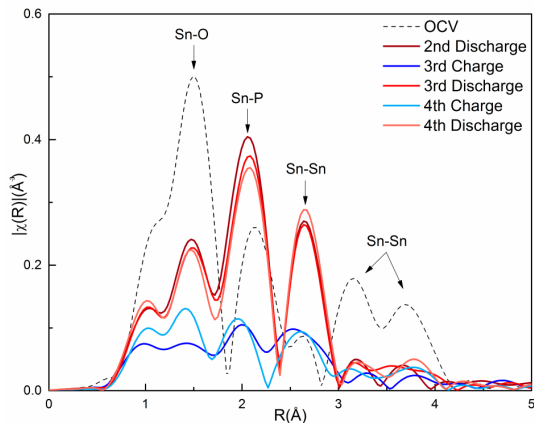
Sn₄P₃/graphite initial cycling



OCV spectrum fits well to Sn₄P₃ structure with an additional Sn-O path

Sn₄P₃ structure persists through first two cycles with possible enhancement of the Sn-Sn path at 2.6 \AA

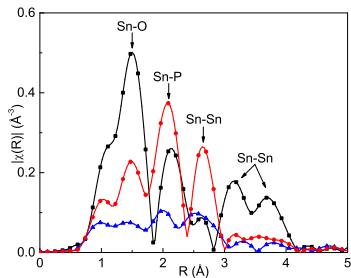
Sn₄P₃/graphite reversible cycling



On third lithiation (charge) the Sn-P path is gone and only Sn-Li remains

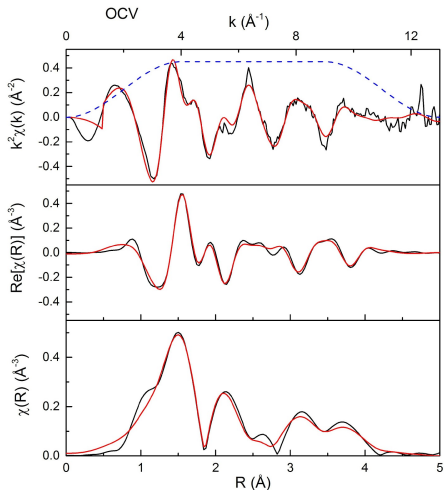
Delithiation (discharge) produces Sn-P and Sn-Sn paths which are not those of Sn₄P₃ but are reversible

Example fits

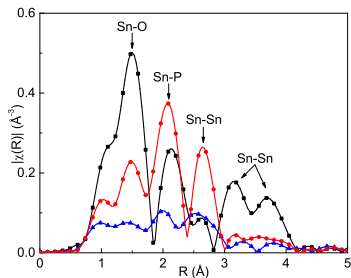


The EXAFS modeling of the Sn_4P_3 /graphite electrode at OCV, 3rd lithiation, and 3rd delithiation, provides bond distances and coordination numbers

The Sn-O peak in the OCV spectrum is primarily due to the ball milling process which inevitably introduces some oxygen.

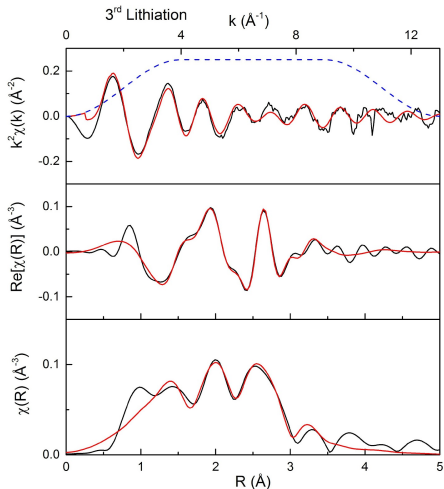


Example fits

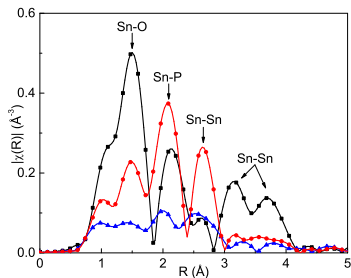


The EXAFS modeling of the Sn_4P_3 /graphite electrode at OCV, 3rd lithiation, and 3rd delithiation, provides bond distances and coordination numbers

By the 3rd lithiated state, the EXAFS is dominated by Sn-Li paths at 2.7 \AA and 3.0 \AA .

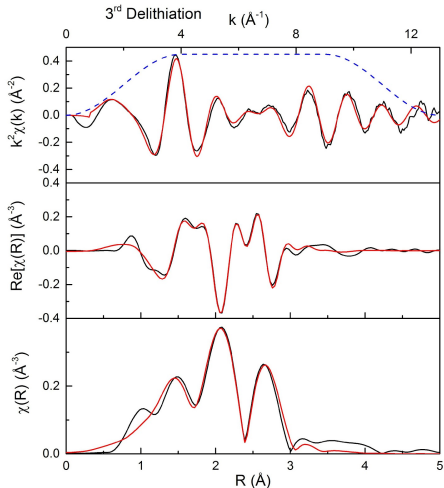


Example fits

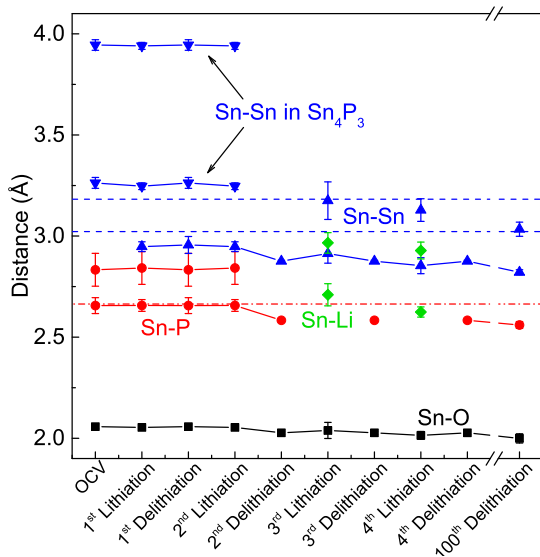


The EXAFS modeling of the Sn_4P_3 /graphite electrode at OCV, 3rd lithiation, and 3rd delithiation, provides bond distances and coordination numbers

At the 3rd delithiation, the Sn-P path reappears but at a shorter distance, in an amorphous SnP_x phase.



Sn₄P₃/graphite path lengths



Sn-Sn distance close to those of metallic Sn indicate the presence of small Sn clusters which may never fully lithiate

Longer Sn-P distance characteristic of Sn₄P₃ is gone after initial conversion to the SnP_x amorphous phase is complete

Only 2 Sn-Li paths present in this material

Sn-O distances remain constant, likely indicative of surface contamination

Sn₄P₃/graphite coordination numbers



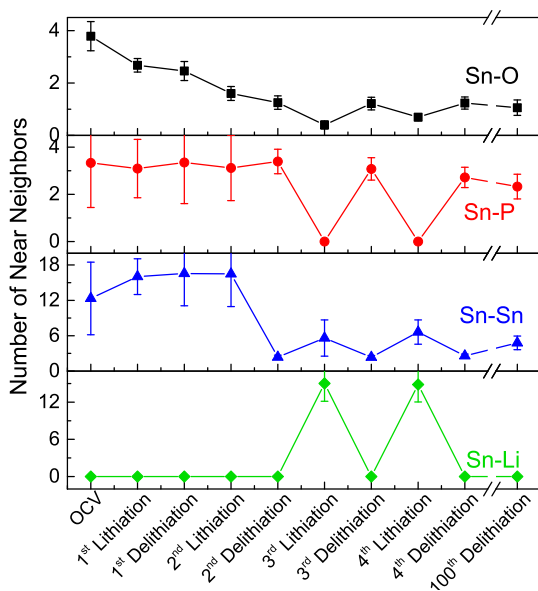
Sn-O neighbors decrease quickly, remaining small and partially reversible up to 100 cycles

Sn-P reversible after initial conversion with a slow decrease which correlates to capacity loss

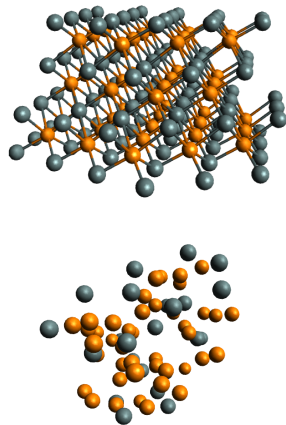
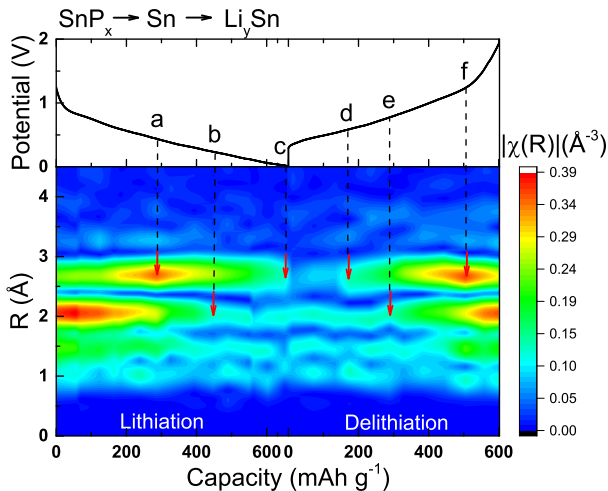
Very small Sn-Sn metallic clusters present throughout

The ~ 3.3 Sn-P neighbors in the delithiated state indicate a possibly tetrahedral Sn coordination in SnP_x

15 Sn-Li neighbors correspond to nearly full lithiation and fade with capacity.



Third cycle dynamic snapshot



Y. Ding et al., "In situ EXAFS-derived mechanism of highly reversible tin phosphide/graphite composite anode for Li-ion batteries," *Adv. Energy Mater.* **2017**, 1702134 (2017).



Elena Timofeeva – Illinois Tech

Initial Sn-based anode studies

Chris Pelliccione – Illinois Tech



Sn₄P₃/graphite composite

Yujia Ding – Illinois Tech

Zhefei Li – Ohio University



Ni@Co core-shell aqueous cathode

Elahe Moazzen – Illinois Tech



Duchossois Leadership Program at
Illinois Tech